Research Article

Nano Biomed Eng

Chloramphenicol and Gentamycin-encapsulated Iron Oxide Nanoparticles as a Nanocarrier for Antibacterial Efficacy via Targeted Drug Delivery

Vandana Sharma[1], J. K. Sharma[1], Vishal Kansay[1], Varun Dutt Sharma[1], Rekha Sheoran[1], Manoj Singh[2], Chhavi Pahwa[1], Anupam Sharma[3], Suresh Kumar[1], A. K. Sharma[2], M. K. Bera[1]

[1] Department of Physics, MM Engineering College, Maharishi Markandeshwar (deemed to be University), Haryana 133207, India
[2] Department of Biotechnology, MM Engineering College, Maharishi Markandeshwar (deemed to be University), Haryana 133207, India
[3] MMIS, Maharishi Markandeshwar (deemed to be University), Haryana 133207, India

Corresponding author. E-mail: m.k.bera@mmumullana.org

Received: Feb. 13, 2023; **Revised:** Jun. 10, 2023; **Accepted:** Jun. 25, 2023

Citation: V. Sharma, J.K. Sharma, M.K. Bera, et al. Chloramphenicol and gentamycin-encapsulated iron oxide nanoparticles as a nanocarrier for antibacterial efficacy via targeted drug delivery. *Nano Biomedicine and Engineering*, 2023, 15(2): 170−178.

http://doi.org/10.26599/NBE.2023.9290029

Abstract

Surface functionalization of iron oxide nanoparticles (Fe_2O_3 NPs) with antibiotics is a novel approach that opens the door to drug delivery applications. In the present work, we report iron oxide nanoparticles synthesized by chemical co-precipitation method. As-synthesized nanoparticles were characterized using field emission scanning electron microscopy (FESEM) , energy dispersive X-ray (EDX), X-ray diffraction (XRD), ultraviolet (UV)–visible (Vis) spectroscopy, Fourier transform infrared (FTIR), and vibrating sample magnetometer (VSM). The poly-shaped Fe_2O_3 NPs of size (34 ± 10) nm with hematite (α-Fe_2O_3) phase were synthesized. The antibacterial activity of chloramphenicol and gentamicin and their formulation with encapsulated iron oxide nanoparticles was investigated by the agar well diffusion technique. Drug-encapsulated Fe_2O_3 NPs showed antibacterial activity against *Escherichia coli* and *Staphylococcus aureus* strains, possibly in a dose-dependent manner. Significant effectiveness was confirmed by the increase in the single range of inhibition against the tested microorganisms. Furthermore, the effect of iron oxide nanoparticle concentrations ranging from 1 to 9 μg/μL on bacterial growth was examined.

Keywords: iron oxide nanoparticles (Fe_2O_3 NPs); antibacterial efficacy; biomimetic; drug delivery systems; chloramphenicol; gentamycin

Introduction

The rise of antibiotic-resistant bacterial types has made fighting illnesses more difficult. To address this, scientists are seeking for better and more effective antibacterial agents. Many studies have reported on nanoparticles and their antimicrobial properties [1–6]. Metal oxides have been gained prominence in biomedical applications due to their high efficiency and ability to be tailored in size and form [7–10]. Drug delivery in the form of nanoparticles has several advantages that outweigh those of conventional drug delivery techniques. Iron oxide nanoparticles as part of a nanodrug delivery system have an advantage over others due to their remarkable properties such as strong

superparamagnetism and a larger easily tunable surface area. It also helps to achieve site-specific drug delivery, which helps to overcome the challenges and concerns of desired bioavailability and further helps in the elimination of malignant cells. The special properties and various ways of creating such nanoparticles have allowed them to be widely used in many applications [11–13].

Using the magnetic and biological features of iron oxide nanocarriers to bind or load drugs has shown to be an efficient technique to boost the therapeutic efficacy of these drugs. The majority of drugs can have their inappropriate properties such as, poor solubility, high toxicity, nonspecific binding, and brief circulation half-lives, which may be overcome by being conjugated to iron oxide nanoparticles [14–16]. In addition to exceptional magnetic capabilities, iron oxide nanoparticles (Fe_2O_3 NPs) are biocompatible, stable and environmentally friendly, making them a suitable platform for biomedical applications. In addition, these nanocarriers are non-toxic, biodegradable, biocompatible and efficiently removed from the human body through iron metabolism. Several drugs have been combined with iron oxide nanoparticles to improve its antibacterial properties [17–19].

In this study, we have reported the synthesis of Fe_2O_3 NPs conjugated with drugs, chloramphenicol and gentamicin and compared its antimicrobial property without Fe_2O_3 NPs.

Experimental

Materials

Iron (III) chloride hexahydrate ($FeCl_3 \cdot 6H_2O$), iron(II) sulfate heptahydrate ($FeSO_4 \cdot 7H_2O$), and sodium hydroxide (NaOH) were obtained from Sisco Research Laboratories Pvt. Ltd. (India) and used as such without further purification. The bacterial culture media, nutrients broth, and nutrient agar were purchased from Hi Media, Mumbai, India. Other materials were purchased from a commercial supplier included Whatman filter paper (grade 1), acetone, ethanol, and isopropyl alcohol. Deionized water was obtained using a Milli-Q system (18.2 $M\Omega \cdot cm^{-1}$, Millipore, France). The deionized water was used for the preparation of reagents and culture media. The two different drugs used in this study were chloramphenicol and gentamycin. The bacterial isolates used for this study were procured from the Microbial Type Culture Collection (MTCC). They are *Staphylococcus aureus* (MTCC – 737), and *Escherichia coli* (MTCC – 739).

Synthesis of iron oxide nanoparticles

The chemical co-precipitation method was used for the synthesis of Fe_2O_3 NPs. Briefly, 2.7 g of iron (III) chloride hexahydrate ($FeCl_3 \cdot 6H_2O$) and 1.39 g of iron(II) sulfate heptahydrate ($FeSO_4 \cdot 7H_2O$) were dissolved in 50 mL of deionized water separately under continuous stirring at room temperature to prepare homogeneous solutions of 0.2 mol/L iron (III) chloride and 0.1 mol/L iron(II) sulfate solution, respectively. The two solution were then mixed together under continuous stirring at room temperature (300 K). 1.0 mol/L NaOH was added dropwise with continuous stirring at 600 r/min to elevate the pH of the solution to 12, resulting in a black precipitate. It was then held for a few hours to stabilize. The precipitate was removed from the solution by centrifuging it for 10 min at 6 000 r/min, and the resultant Fe_2O_3 NPs were carefully washed with distilled water before drying overnight in a hot air oven at 60 °C. The nanopowder was then calcinated at 500 °C for 3 h in a hot furnace. Dried Fe_2O_3 NPs powder was utilized for additional analytical and physical characterization.

Characterizations and Instrumentations

The ultra-centrifugation of the sample was done with REMI CPR-30 Plus centrifuge machine. The ultraviolet (UV)–visible (Vis) absorption spectra were taken with a Shimadzu UV-2600 spectrophotometer for solid samples and a Molecular Devices SpectraMax iD3 spectrophotometer for liquid samples, with a step of 1 nm in the wavelength ranges of 200–800 nm. The stirring of the sample was done using a REMI MS-500 magnetic stirrer. The nature of surface functionalization was assessed using a Shimadzu IR Spirit Fourier transform infrared (FTIR) spectrophotometer in the wavelength rang of 4 000–400 cm^{-1}. The crystalline nature of the Fe_2O_3 NPs was determined using a Bruker D8 Advance diffractometer at 40 kV, 40 mA, and a non-monochromatic CuK_α X-ray with an angular range (2θ) of 5°–90° and an angular step of 0.02°. The morphologies of as-synthesized Fe_2O_3 NPs were investigated using a Zeiss field emission scanning

electron microscope (FESEM) with an accelerating voltage of 5 kV. The energy-dispersive X-ray spectroscopy (EDX) was used to evaluate the composition of as-synthesized Fe_2O_3 NPs. Magnetization measurement was performed at room temperature using a vibrating sample magnetometer (VSM-7404, Lake Shore, USA).

Bacterial reduction assay

Microbial assays were used to evaluate the effectiveness of the investigated iron oxide-coated antibiotics (chloramphenicol and gentamicin) by comparing the inhibition of the growth of sensitive bacteria produced by known amounts of the test antibiotic and a reference drug. Being the most prevalent species of Gram-negative and Gram-positive bacteria, *E. coli* and *S. aureus*, respectively were inoculated and incubated overnight at 37 °C in a nutrient broth for 24 h to study the bacterial growth curve. A spectrophotometer was used to evaluate bacterial growth curves by measuring the optical density (OD) at 620 nm. Activity was tested at various time intervals ranging from 1 to 28 h at incubation concentrations of 1–9 μg/μL [20].

Preparation of antibiotic-coated Fe_2O_3 NPs

Nanomedicine for antibiotic delivery can increase the effectiveness of antibacterial therapy. Nanosystems for antibiotic delivery and targeting infection sites have a number of advantages over conventional formulations. Antibiotic-protected Fe_2O_3 NPs were prepared to investigate the role of nanoparticles in microbial activity. For this purpose, drug-coated Fe_2O_3 NPs were prepared by mixing nanoparticles (10 cm^3 of 1 mmol/L Fe_2O_3) with 10 cm^3 of 1 mmol/L drug diluted in 50 mL of double-distilled water and stirred vigorously for 2 h. This is designated as a control sample. The two drugs used in this study were chloramphenicol and gentamicin. The bacterial isolates used in this study were *S. aureus* and *E. coli*.

Microbial assay

Bacterial sensitivity to drugs coated with bioconjugated nanoparticles was investigated using an agar disk diffusion test. Drug-coated Fe_2O_3 NPs were placed on agar plates and left at 25 °C for 1 h to allow pre-incubation diffusion to reduce the effect of time differences when different solutions were used. After 24 h of incubation at 37 °C, the plates were examined for antibacterial activity by measuring the width of the inhibition zones for each bacterial culture.

Assessment of increase in fold area

To estimate the fold area increase, the mean surface area of the inhibitory zone of pure drugs and drugs coated with Fe_2O_3 NPs was determined. The fold increase area of each tested bacteria was calculated by the equation: $(B^2 - A^2)/A^2$, where A and B were the zones of inhibition for prescription drugs and drugs coated with Fe_2O_3 NPs, respectively [21].

Results and Discussion

Structural, morphological and chemical characteristics of Fe_2O_3 NPs

The morphology of the synthesized Fe_2O_3 NPs is shown in Fig. 1(a). The figure shows that the synthesized Fe_2O_3 NPs are not homogeneous in nature and, in some circumstances, agglomerate. The particles are found to be polygon in nature with a size distribution within the range of (34 ± 10) nm, as illustrated in Fig. 1(b). The large agglomerated clusters developed as a result of the accumulation of microscopic reducing agent building blocks, or it might be owing to a lack of capping layer.

Furthermore, due to the high surface area to volume ratio and the strong Van der Waals attractive interactions, and magnetic forces, magnetic nanoparticles tend to agglomerate and form massive clusters, resulting in increased particle size.

EDX analysis was also used to determine the elemental composition of the Fe_2O_3 NPs. The EDX analysis in Fig. 1(c) clearly shows the presence of corresponding L_α at 0.7 and K_α about 6.4 keV due to the presence of Fe atoms in the nanoparticle, as well as another K_α line at 0.6 keV due to the presence of O atoms. The atomic proportion of mass present in the irradiated area is 19.38% for iron and 80.62% for oxygen, respectively (Table in Fig. 1(c)). It is noteworthy that the observed carbon from EDX spectra (CK_α at 0.2 keV) may come from organic solvents, or supporting grid utilized. Any organic contamination tends to produce hydrocarbon on the sample surface under the electron beam, the amount of which might rise during the measurement.

Besides, a tiny peak detected at around 2.3 keV is associated with sulfur impurity (S K_α), which is likely

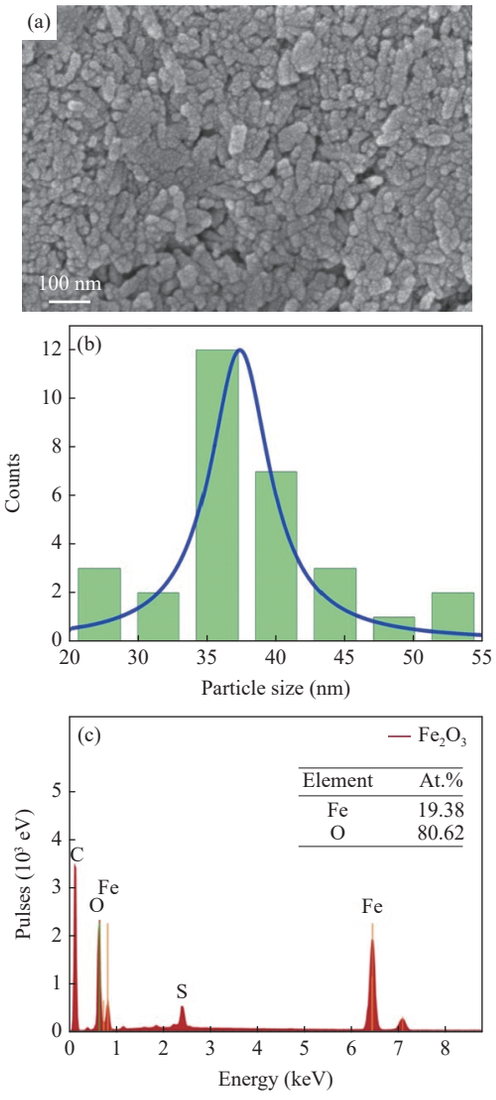

Fig. 1 (a) FESEM micrograph of chemically synthesized Fe_2O_3 NPs. The scale bar corresponds to 100 nm. (b) Fe_2O_3 NPs size distribution histogram. (c) EDX spectral analysis of chemically synthesized Fe_2O_3 NPs.

to arise from iron(II) sulfate heptahydrate precursor.

Furthermore, the presence of functional groups and the formation of Fe_2O_3 NPs in the prepared samples were determined by FTIR spectra. The FTIR spectra of as-synthesized and calcined Fe_2O_3 NPs are shown in Fig. 2.

The FTIR analysis (400–4 000 cm^{-1}) of both as-synthesized Fe_2O_3 NPs confirmed the synthesis of Fe_2O_3 NPs as well as the presence of different reducing agent functional groups associated with Fe_2O_3 NPs (Fig. 2). The spectra of Fe_2O_3 NPs shows two sharp band at 442 and 570 cm^{-1}, which are related to Fe–O vibrations for iron oxide. The weak vibration monitored at 1 073 cm^{-1} is characteristic of surface Fe–OH groups [22]. Other stretching vibrations have been observed at 1 002 cm^{-1} owing to –COO–,

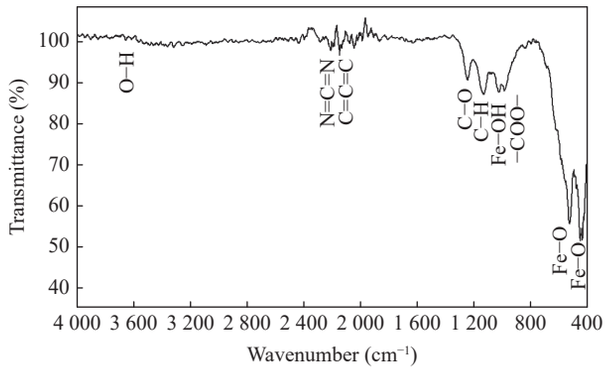

Fig. 2 FTIR spectra of chemically synthesized Fe_2O_3NPs.

1 226 cm^{-1} due to C–H, 1 130 cm^{-1} due to C–O, 2 141 cm^{-1} due to C=C=C, and 2 223 cm^{-1} due to N=C=N [23,24].

The XRD patterns of as-synthesized Fe_2O_3 NPs is shown in Fig. 3(a). X-ray diffraction reveals the development of polycrystalline iron oxide nanoparticles with strong peaks from the (012), (104), (110), (113), (024), (116), (018), (214), and (300) planes which can be indexed to hematite (α-Fe_2O_3) having hexagonal configuration (JCPDS Card No. 86–0550). It is worth noting that the three most common forms of iron oxides found in nature are magnetite (Fe_3O_4), maghemite (γ-Fe_2O_3), and hematite (α-Fe_2O_3); however, XRD makes distinguishing the presence of magnetite (Fe_3O_4) and maghemite (γ-Fe_2O_3) difficult because magnetite and maghemite have nearly identical crystal structures. Hematite is the most stable form of iron oxide among these crystalline phases. Hematite nanoparticles usually can be produced using a variety of processes, including chemical co-precipitation, hydrothermal synthesis, and the sol–gel approach [25]. The particle size and morphology of these nanoparticles can be easily tailored by controlling various parameters specific to their route of synthesis.

On the other hand, the average crystallite size (d_{cryl}) was calculated using the prominent peaks from Debye–Scherrer formula [26]: $d_{cryl} = \frac{\kappa\lambda}{\beta\cos\theta}$, where κ is a constant (0.9 for spherical shape), λ is the wavelength of CuK_α radiation (0.15406 nm), β is the full width at half maximum (FWHM) of the diffraction peak in radians and θ is the Bragg's diffraction angle, respectively. The estimated average crystallite sizes were found to be around 21.9 nm. Furthermore, the lattice strain was derived from the FWHM of the diffraction peaks using the Williamson–Hall (W–H) plot and the following relationship [26]:

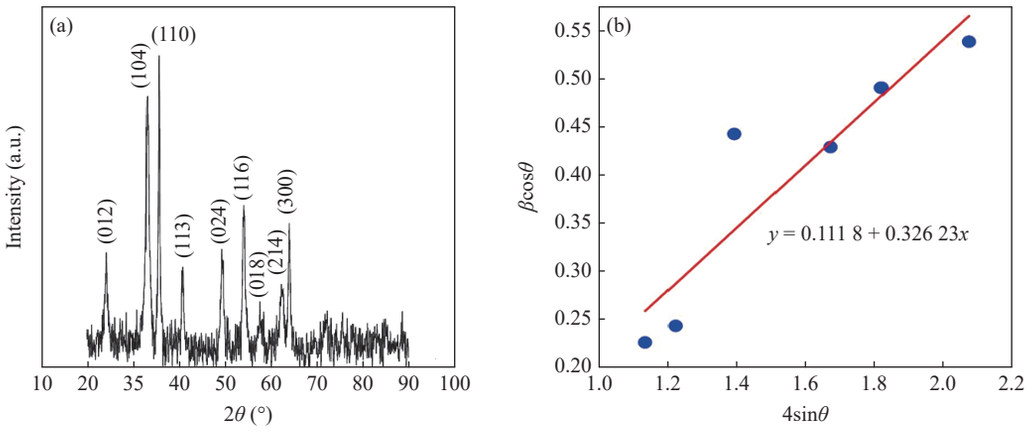

Fig. 3 (a) X-ray diffraction patterns and (b) W–H plot from the obtained XRD data of as-synthesized Fe_2O_3 NPs.

$$\beta\cos\theta = \frac{\kappa\lambda}{d_{cryl}} + 4\varepsilon sin\theta \quad (1)$$

where κ is a constant (0.9 for spherical shape), λ is the wavelength of CuK_α radiation (0.15406 nm), β is the FWHM of the diffraction peak in radians and θ is the Bragg's diffraction angle, d_{cryl} is the crystallite size and ε is the effective strain, respectively. For the preferred orientation peaks of Fe_2O_3 NPs, the term ($\beta\cos\theta$) is plotted with respect to ($4\sin\theta$), and the y-intercept and slope of the fitted line determine the crystallite size and associated strain, respectively [27, 28]. The W–H plots in Fig. 3(b) for as-synthesized Fe_2O_3 NPs demonstrate that the strain is extremely modest.

Optical characteristics of Fe_2O_3 NPs

The absorbance spectrum of the as-synthesized Fe_2O_3 NPs by chemical co-precipitation method is shown in Fig. 4. The absorbance peak around 300 nm in Fig. 4 confirmed the formation of Fe_2O_3 NP with indirect optical band gap [29].

Magnetization measurement Fe_2O_3 NPs

The magnetic characteristics of the synthesized Fe_2O_3 NPs were investigated using a vibrating sample magnetometer (VSM). The measurements were taken at room temperature. The magnetization curve (M–H loop) of as-synthesized Fe_2O_3 NPs produced by chemical method is shown in Fig. 5 at a maximum field of 10 kOe. The well-measured hysteresis loop validates its magnetic behavior. However, maximum magnetisation (M_s = 0.5 emu/g) value is small presumably due to lack of sufficient calcination. Furthermore, the obtained relative low coercivity (H_c less than 100 Oe) verifies the soft magnetic character of Fe_2O_3 NPs [29].

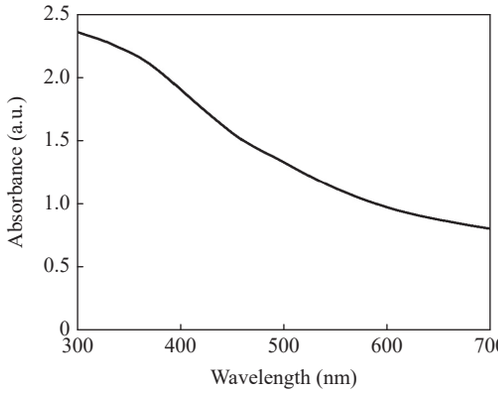

Fig. 4 UV–Vis absorption spectra of chemically synthesized Fe_2O_3 NPs.

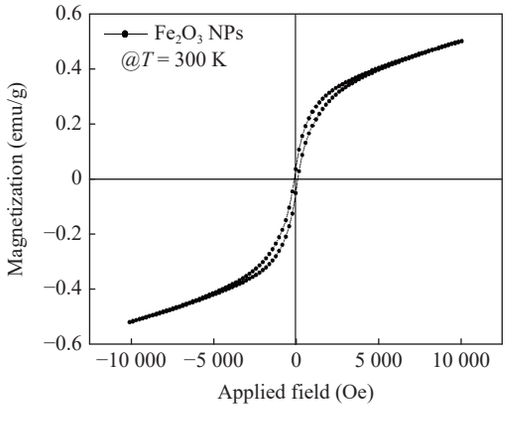

Fig. 5 Magnetic properties (M–H hysteresis curve) of chemically Fe_2O_3 NPs.

Bacterial growth inhibition assay and drug delivery applications of Fe_2O_3 NPs

The bacterial growth inhibitory activity of iron oxide nanoparticles against multi drug resistant strains of Gram-negative (*E. coli*) and Gram-positive (*S. aureus*) bacteria was studied using a bacterial reduction assay at various time intervals ranging from 1 to 28 h. and at different concentrations in the range of 1–9 μg/μL, as shown in Fig. 6.

Antibacterial activities were enhanced when gentamycin and chloramphenicol coated Fe_2O_3 NPs

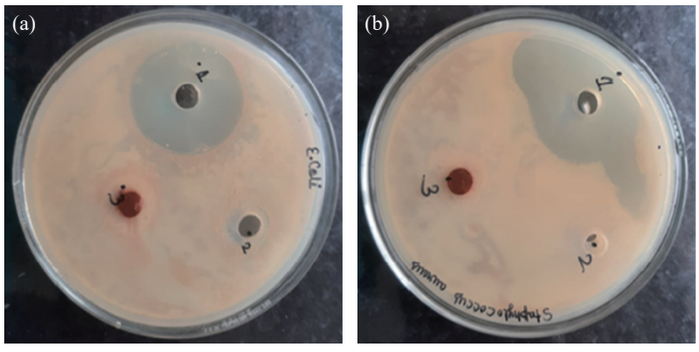

Fig. 6 Antibacterial activity of the drug loaded iron oxide nanoparticles against (a) Gram-negative (*E. coli*) and (b) Gram-positive (*S. aureus*) bacteria.

were utilized as drug carriers, since it is essentially a compound consisting of closely similar aminoglycosides and a family of antimicrobials that normally inhibits protein synthesis (Fig. 6). The primary mechanism of action of these medications is the suppression of protein production or genetic translation. Gentamycin, when coupled with iron, produces phospholipids [30]. It creates a coating surrounding the nanoparticles, with the sulphate group forming a covalent link [31]. The conjugate then participates in cell annihilation by primarily two mechanisms: first, by interfering with protein synthesis, and second, by generating damage to cell membranes. As a result, it gives birth to a very effective drug carrier [32]. It has been observed that all of the examined species showed Fe_2O_3 NPs dose-dependent inhibitory effect. It is anticipated that due to increased surface area, chemical stability and appropriate size of the synthesized NPs, Fe_2O_3 NPs coated with chloramphenicol and gentamycin antibiotic becomes an effective drug carriers. Chloramphenicol or gentamycin antibiotics with or without Fe_2O_3 NPs encapsulated were tested *in vitro* against *E. coli* and *S. aureus*, as illustrated in Figs. 7 and 8, respectively. As shown in Fig. 7, the zone of inhibition for the chloramphenicol drug coated with Fe_2O_3 NPs increased when compared to the drug alone. Similar results were also observed for gentamycin drug coated Fe_2O_3 NPs as can be seen from Fig. 8. As a result of the preceding investigations, it is obvious that both chloramphenicol and gentamycin drug coated iron oxide nanoparticles were extremely efficient against both Gram-positive and Gram-negative bacteria, as evidenced by a greater fold increase in the zone of inhibition diameter.

On the other hand, the Fe_2O_3 NPs had no adverse or side effects on the microbial activities. Hence, this

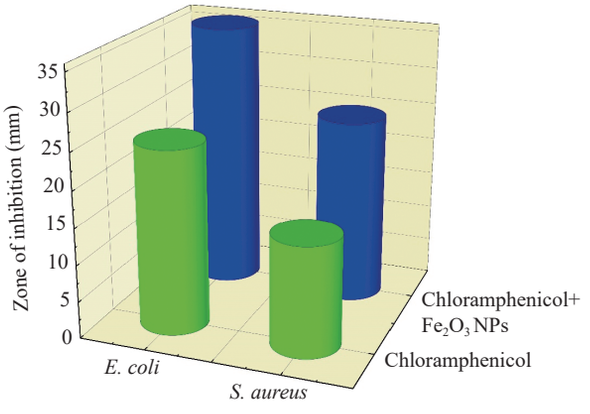

Fig. 7 Zone of inhibition observed using the chloramphenicol-coated Fe_2O_3 NPs. There was a significant inhibition observed in both the bacterial strains using the drug coated nanoparticles in comparison to the drug alone.

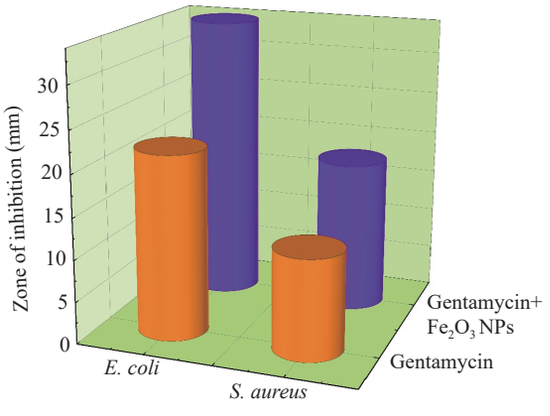

Fig. 8 Gentamycin-coated Fe_2O_3 NPs produced an inhibitory zone. The drug-coated nanoparticles inhibited both bacterial strains significantly and more effectively than the antibiotic alone.

feature of Fe_2O_3 NPs as an effective drug carrier might be further explored for drug delivery systems. Although the mechanism of contact between nanoparticles and the constituents of microorganisms' outer membrane remains unknown, it is probable that the particles interact with the outer membrane's building parts may cause structural alterations or deterioration. In our opinion, the mechanism(s) of

possible enhancement of the antibacterial activity of iron oxide nanoparticle conjugates is still an open question and needs further studies.

Effect of concentration of Fe_2O_3 NPs on bacterial growth

The effect of iron oxide nanoparticle concentration on Gram-positive and Gram-negative bacteria has also been examined. The bacterial growth and optical density values measured at different time intervals (1–28 h) employing varying quantities of Fe_2O_3 NPs in the nutritional broth medium (herein denoted as control) containing *E. coli* are depicted in Figs. 9 and 10. A slight decline in optical density (OD) at 620 nm has been found with increasing concentration of nanoparticles in the nutritional broth medium where bacteria are inoculation, which correlates directly to lower bacterial growth.

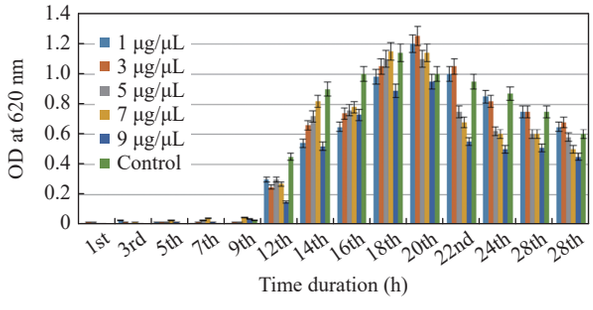

Fig. 9 The figure elucidates the statistical distribution of optical density values observed at different time intervals (1–28 h) using different concentrations of Fe_2O_3 NPs in the nutrient broth medium containing *E. coli.*

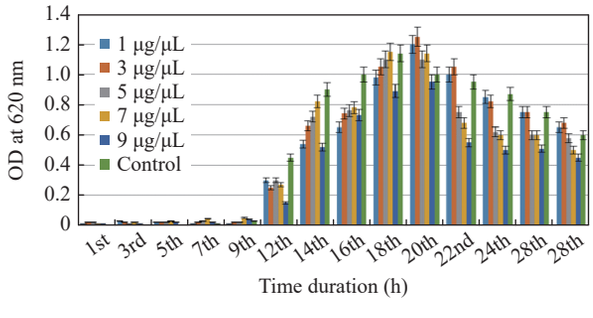

Fig. 10 The statistical distribution of optical density values observed at different time intervals (1–28 h) using different concentrations of Fe_2O_3 NPs in the nutrient broth medium containing *S. aureus.*

A comparison study of bacterial growth under normal and iron oxide nanoparticle conditions indicated the effect of iron nanoparticle on bacterial growth. Under normal conditions, the growth curve of *E. coli* clearly represented the lag- log, stationary, and death phases, as shown in Fig. 9, but under the effect of different concentrations of Fe_2O_3 NPs, the growth curve was deformed (i.e., 1, 3, 5, 7, and 9 µg/µL) The gradual shortening of log phase was observed, demonstrating that iron nanoparticles have a micro biostatic effect on *E. coli* in a concentration dependent way. In the case of iron oxide (3 µg/µL) treated bacterial cells, the untreated bacterial sample reached OD_{620} at the 20th hour (Fig. 9). The inhibition is assumed to be caused by reactive oxygen species (ROS), superoxide radicals ($O_2^{\bullet-}$), hydroxide radicals (•OH), and singlet oxygen ($^1O_2$) produced by the Fe_2O_3 NPs [33]. ROS generation has been identified in a wide variety of metal oxide nanoparticles, which may cause oxidative stress, inflammation, and subsequent damage to proteins, membranes, and DNA, which is one of the key causes of nanotoxicity.

Similar observations have also been found for *S. aureus*. Fig. 10 depicts the optical density values obtained at various time intervals (1–28 h) using varying quantities of Fe_2O_3 NPs in the nutritional broth medium containing *S. aureus*.

The OD measurements as shown in Fig. 10 revealed that the presence of Fe_2O_3 NPs had no effect on the quantity of bacteria. However, and more importantly, the live/dead assay results showed that after 12–14 h, the ratio of live/dead bacteria was significantly lower in the solution with the highest dose (9 µg/µL) of Fe_2O_3 NPs compared to the control sample, as well as the low and medium dose samples; the same trend was observed after 12 and 24 h. Several factors contributed to the bactericidal properties of the currently researched Fe_2O_3 NPs [34]. ROS-induced oxidative stress is the primary mechanism through which antibacterial medicines and antibiotics work [35]. ROS, which include superoxide radicals, hydroxyl radicals, hydrogen peroxide (H_2O_2), and singlet oxygen ($^1O_2$), can harm bacteria's proteins and DNA. In this investigation, the concentration of nanoparticles made a significant impact to the reduction of *S. aureus* activity. Kim *et al.* discovered a similar concentration-dependent trend while studying the antibacterial activities of iron oxide nanoparticles on *S. aureus* and *E. coli* [36, 37]. Therefore from the above-mentioned discussion, it is clear that iron oxide nanoparticles is reasonable well suited for antibacterial efficacy and drug delivery.

Conclusion

In this study, nano scaled Fe_2O_3 NPs were synthesized under atmospheric conditions utilizing a simple chemical co-precipitation process including ferric chloride and ferrous sulfate. Comprehensive analysis of iron oxide nanoparticles employing FESEM, EDX, XRD, FTIR, UV–Vis, and VSM investigations confirmed their synthesis. Polyshaped Fe_2O_3 with a diameter of (34 ± 10) nm were created. At ambient temperature, the magnetic properties of the generated Fe_2O_3 NPs were studied using a VSM with a very weak magnetisation value of (M_s = 0.5 emu/g). The synthesized drug-encapsulated (gentamycin and chloramphenicol) nanoparticles showed antibacterial activity against the *E. coli* and *S. aureus* bacterial strains putatively exhibiting effects in a dose dependent manner. The effect of iron oxide nanoparticle concentration on both Gram-positive and Gram-negative bacteria has also been examined. There is a minor drop in OD at 620 nm with increasing nanoparticle content in the nutrient broth medium containing *E. coli* and *S. aureus*. Due to advancements in the field of surface chemistry, assessing the chemical stability and appropriate size of the synthesized NPs, it becomes of paramount interest to develop Fe_2O_3 NPs and explore them further using the antibiotics coated composites as an effective drug carrier.

CRediT Author Statement

Vandana Sharma: Investigation, formal analysis, and writing. **J. K. Sharma:** Conceptualization, investigation, and methodology. **Vishal Kansay:** Investigation, formal analysis, methodology, and writing. **Varun Dutt Sharma:** Investigation, formal analysis, methodology, and writing. **Rekha Sheoran:** Investigation, methodology, and formal analysis. **Manoj Singh:** Investigation, methodology, and formal analysis. **Chhavi Pahwa:** Investigation and formal analysis. **Anupam Sharma:** Investigation. **Suresh Kumar:** Investigation. **M. K. Bera:** Conceptualization, investingigation, methodology, writing-reviewing and editing, and overall supervision.

Conflict of Interest

The authors declare that no competing interest exists.

References

[1] M. Ramezani Farani, M. Azarian, H. Heydari Sheikh Hossein, et al. Folic acid-adorned curcumin-loaded iron oxide nanoparticles for cervical cancer. *ACS Applied Bio Materials*, 2022, 5(3): 1305−1318. https://doi.org/10.1021/acsabm.1c01311

[2] R.L. Siegel, K.D. Miller, H.E. Fuchs, et al. Cancer statistics, 2022. *CA*: *a Cancer Journal for Clinicians*, 2022, 72(1): 7−33. https://doi.org/10.3322/caac.21708

[3] M. Ebadi, K. Buskaran, S. Bullo, et al. Drug delivery system based on magnetic iron oxide nanoparticles coated with (polyvinyl alcohol-zinc/aluminium-layered double hydroxide-sorafenib). *Alexandria Engineering Journal*, 2021, 60(1): 733−747. https://doi.org/10.1016/j.aej.2020.09.061

[4] L.M. Ngema, S.A. Adeyemi, T. Marimuthu, et al. Synthesis of novel conjugated linoleic acid (CLA)-coated superparamagnetic iron oxide nanoparticles (SPIONs) for the delivery of paclitaxel with enhanced *in vitro* anti-proliferative activity on A549 lung cancer cells. *Pharmaceutics*, 2022, 14(4): 829. https://doi.org/10.3390/pharmaceutics14040829

[5] T. Vangijzegem, D. Stanicki, S. Laurent. Magnetic iron oxide nanoparticles for drug delivery: Applications and characteristics. *Expert Opinion on Drug Delivery*, 2019, 16(1): 69−78. https://doi.org/10.1080/17425247.2019.1554647

[6] M. Sharaf, A.H. Sewid, H.I. Hamouda, et al. Rhamnolipid-coated iron oxide nanoparticles as a novel multitarget candidate against major foodborne E. coli serotypes and methicillin-resistant S. aureus. *Microbiol Spectr*, 2022, 10(4): e0025022. https://doi.org/10.1128/spectrum.00250-22

[7] S.A. Sankaranarayanan, A. Thomas, N. Revi, et al. Iron oxide nanoparticles for theranostic applications - Recent advances. *Journal of Drug Delivery Science and Technology*, 2022, 70: 103196. https://doi.org/10.1016/j.jddst.2022.103196

[8] A. Mengesha, A. Hoerres, P. Mahajan. Cytocompatibility of oleic acid modified iron oxide nanoparticles. *Materials Letters*, 2022, 323: 132528. https://doi.org/10.1016/j.matlet.2022.132528

[9] J. Dulińska-Litewka, A. Łazarczyk, P. Hałubiec, et al. Superparamagnetic iron oxide nanoparticles-current and prospective medical applications. *Materials* (*Basel*, *Switzerland*), 2019, 12(4): E617. https://doi.org/10.3390/ma12040617

[10] P. Sangaiya, R. Jayaprakash. A review on iron oxide nanoparticles and their biomedical applications. *Journal of Superconductivity and Novel Magnetism*, 2018, 31(11): 3397−3413. https://doi.org/10.1007/s10948-018-4841-2

[11] S.V. Gudkov, D.E. Burmistrov, D.A. Serov, et al. Do iron oxide nanoparticles have significant antibacterial properties? *Antibiotics* (*Basel*, *Switzerland*), 2021, 10(7): 884. https://doi.org/10.3390/antibiotics10070884

[12] S. Belaïd, D. Stanicki, L. Vander Elst, et al. Influence of experimental parameters on iron oxide nanoparticle properties synthesized by thermal decomposition: Size and nuclear magnetic resonance studies. *Nanotechnology*, 2018, 29(16): 165603. https://doi.org/10.1088/1361-6528/aaae59

[13] M. Khatami, H.Q. Alijani, B.A. Fakheri, et al. Super-paramagnetic iron oxide nanoparticles (SPIONs): Greener synthesis using Stevia plant and evaluation of its antioxidant properties. *Journal of Cleaner Production*, 2019, 208: 1171−1177. https://doi.org/10.1016/j.jclepro.2018.10.182

[14] S.M. Dadfar, K. Roemhild, N.I. Drude, et al. Iron oxide nanoparticles: Diagnostic, therapeutic and theranostic applications. *Advanced Drug Delivery Reviews*, 2019,

138: 302−325. https://doi.org/10.1016/j.addr.2019.01.005
[15] P. Bender, J. Fock, M.F. Hansen, et al. Influence of clustering on the magnetic properties and hyperthermia performance of iron oxide nanoparticles. *Nanotechnology*, 2018, 29(42): 425705. https://doi.org/10.1088/1361-6528/aad67d
[16] A. Elsaidy, J.P. Vallejo, V. Salgueiriño, et al. Tuning the thermal properties of aqueous nanofluids by taking advantage of size-customized clusters of iron oxide nanoparticles. *Journal of Molecular Liquids*, 2021, 344: 117727. https://doi.org/10.1016/j.molliq.2021.117727
[17] S. Parveen, A.H. Wani, M.A. Shah, et al. Preparation, characterization and antifungal activity of iron oxide nanoparticles. *Microbial Pathogenesis*, 2018, 115: 287−292. https://doi.org/10.1016/j.micpath.2017.12.068
[18] A.V. Nikam, B.L.V. Prasad, A.A. Kulkarni. Wet chemical synthesis of metal oxide nanoparticles: A review. *CrystEngComm*, 2018, 20(35): 5091−5107. https://doi.org/10.1039/C8CE00487K
[19] Zhu, N., Ji, H. N., Yu, P., Niu, J. Q., Farooq, M., Akram, M., Udego, I., Li, H. D., Niu, X. B. Surface modification of magnetic iron oxide nanoparticles. *Nanomaterials*, 2018, 8(10): 810. https://doi.org/10.3390/nano8100810
[20] M. Singh, S. Manikandan, M. Yadav, et al. Bio-functionalized gold nanoparticles: A potent probe for profound antibacterial efficiency through drug delivery system. *Asian Journal of Biological and Life Sciences*, 2020, 9(2): 139−144. https://doi.org/10.5530/ajbls.2020.9.21
[21] S.S. Birla, V.V. Tiwari, A.K. Gade, et al. Fabrication of silver nanoparticles by*Phoma glomerata*and its combined effect against*Escherichia coli*, *Pseudomonas aeruginosa*and*Staphylococcus aureus*. *Letters in Applied Microbiology*, 2009, 48(2): 173–179. https://doi.org/10.1111/j.1472-765X.2008.02510.x
[22] N.M. Sundaram, S. Murugesan. Preparation and characterization of an iron oxide-hydroxyapatite nanocomposite for potential bone cancer therapy. *International Journal of Nanomedicine*, 2015: 99. https://doi.org/10.2147/IJN.S79985
[23] S.S. Alias, A.B. Ismail, A.A. Mohamad. Effect of pH on ZnO nanoparticle properties synthesized by Sol–gel centrifugation. *Journal of Alloys and Compounds*, 2010, 499(2): 231−237. https://doi.org/10.1016/j.jallcom.2010.03.174
[24] A.M. Mazrouaa, M.G. Mohamed, M. Fekry. Physical and magnetic properties of iron oxide nanoparticles with a different molar ratio of ferrous and ferric. *Egyptian Journal of Petroleum*, 2019, 28(2): 165−171. https://doi.org/10.1016/j.ejpe.2019.02.002
[25] H.T. Cui, Y. Liu, W.Z. Ren. Structure switch between α-Fe_2O_3, γ-Fe_2O_3 and Fe_3O_4 during the large scale and low temperature Sol-gel synthesis of nearly monodispersed iron oxide nanoparticles. *Advanced Powder Technology*, 2013, 24(1): 93−97. https://doi.org/10.1016/j.apt.2012.03.001
[26] J.P. Mathew, G. Varghese, J. Mathew. Effect of post-thermal annealing on the structural and optical properties of ZnO thin films prepared from a polymer precursor. *Chinese Physics B*, 2012, 21(7): 078104. https://doi.org/10.1088/1674-1056/21/7/078104
[27] A. Kumar, Gangawane K.M. Effect of precipitating agents on the magnetic and structural properties of the synthesized ferrimagnetic nanoparticles by co-precipitation method. *Powder Technology*, 2022, 401: 117298. https://doi.org/10.1016/j.powtec.2022.117298
[28] N. Shabani, A. Javadi, H. Jafarizadeh-Malmiri, et al. Potential application of iron oxide nanoparticles synthesized by Co-precipitation technology as a coagulant for water treatment in settling tanks. *Mining, Metallurgy & Exploration*, 2021, 38(1): 269−276. https://doi.org/10.1007/s42461-020-00338-y
[29] J. Chatterjee, Y. Haik, C.J. Chen. Size dependent magnetic properties of iron oxide nanoparticles. *Journal of Magnetism and Magnetic Materials*, 2003, 257(1): 113−118. https://doi.org/10.1016/S0304-8853(02)01066-1
[30] T.V. Harris, R.K. Szilagyi. Iron–sulfur bond covalency from electronic structure calculations for classical iron–sulfur clusters. *Journal of Computational Chemistry*, 2014, 35(7): 540−552. https://doi.org/10.1002/jcc.23518
[31] P. Bhattacharya, S. Neogi. Gentamicin coated iron oxide nanoparticles as novel antibacterial agents. *Materials Research Express*, 2017, 4(9): 095005. https://doi.org/10.1088/2053-1591/aa8652
[32] R. Safarkar, R.G. Ebrahimzadeh, S. Khalili-Arjagi. The study of antibacterial properties of iron oxide nanoparticles synthesized using the extract of lichen Ramalina sinensis. *Asian Journal of Nanoscience and Materials*, 2020, 3(3): 157−166. https://doi.org/10.26655/AJNANOMAT.2020.3.1
[33] M. Bloemen, C. Denis, M. Peeters, et al. Antibody-modified iron oxide nanoparticles for efficient magnetic isolation and flow cytometric determination of L. pneumophila.*Microchimica Acta*, 2015, 182(7−8): 1439–1446. https://doi.org/10.1007/s00604-015-1466-z
[34] M.A. Kohanski, D.J. Dwyer, B. Hayete, et al. A common mechanism of cellular death induced by bactericidal antibiotics. *Cell*, 2007, 130(5): 797−810. https://doi.org/10.1016/j.cell.2007.06.049
[35] H. Sies. Oxidative stress: Oxidants and antioxidants. *Experimental Physiology*, 1997, 82(2): 291−295. https://doi.org/10.1113/expphysiol.1997.sp004024
[36] L.L. Zhang, Y.H. Jiang, Y.L. Ding, et al. Investigation into the antibacterial behaviour of suspensions of ZnO nanoparticles (ZnO nanofluids). *Journal of Nanoparticle Research*, 2007, 9(3): 479−489. https://doi.org/10.1007/s11051-006-9150-1
[37] J.S. Kim, E. Kuk, K.N. Yu, et al. Antimicrobial effects of silver nanoparticles. *Nanomedicine*: *Nanotechnology*, *Biology and Medicine*, 2007, 3(1): 95−101. https://doi.org/10.1016/j.nano.2006.12.001